doi:10.1016/j.jmb.2009.06.076 J. Mol. Biol. (2009) 392, 1339–1356

JMB

Available online at www.sciencedirect.com

ScienceDirect

ELSEVIER

Pathways and Mechanisms for Product Release in the Engineered Haloalkane Dehalogenases Explored Using Classical and Random Acceleration Molecular Dynamics Simulations

Martin Klvana[1], Martina Pavlova[1], Tana Koudelakova[1], Radka Chaloupkova[1], Pavel Dvorak[1], Zbynek Prokop[1], Alena Stsiapanava[2], Michal Kuty[2,3], Ivana Kuta-Smatanova[2,3], Jan Dohnalek[4], Petr Kulhanek[5], Rebecca C. Wade[6] and Jiri Damborsky[1]*

[1]*Loschmidt Laboratories, Institute of Experimental Biology and National Centre for Biomolecular Research, Faculty of Science, Masaryk University, Kamenice 5/A4, 625 00 Brno, Czech Republic*

[2]*Institute of Physical Biology, University of South Bohemia, Zámek 136, 373 33 Nové Hrady, Czech Republic*

[3]*Institute of Systems Biology and Ecology, Academy of Sciences of the Czech Republic, Zámek 136, 373 33 Nové Hrady, Czech Republic*

[4]*Institute of Macromolecular Chemistry, Academy of Sciences of the Czech Republic, Heyrovského náměstí 2, 162 06 Praha 6, Czech Republic*

[5]*Laboratory of Computational Chemistry, National Centre for Biomolecular Research, Faculty of Science, Masaryk University, Kamenice 5/A4, 625 00 Brno, Czech Republic*

Eight mutants of the DhaA haloalkane dehalogenase carrying mutations at the residues lining two tunnels, previously observed by protein X-ray crystallography, were constructed and biochemically characterized. The mutants showed distinct catalytic efficiencies with the halogenated substrate 1,2,3-trichloropropane. Release pathways for the two dehalogenation products, 2,3-dichloropropane-1-ol and the chloride ion, and exchange pathways for water molecules, were studied using classical and random acceleration molecular dynamics simulations. Five different pathways, denoted p1, p2a, p2b, p2c, and p3, were identified. The individual pathways showed differing selectivity for the products: the chloride ion releases solely through p1, whereas the alcohol releases through all five pathways. Water molecules play a crucial role for release of both products by breakage of their hydrogen-bonding interactions with the active-site residues and shielding the charged chloride ion during its passage through a hydrophobic tunnel. Exchange of the chloride ions, the alcohol product, and the waters between the buried active site and the bulk solvent can be realized by three different mechanisms: (i) passage through a permanent tunnel, (ii) passage through a transient tunnel, and (iii) migration through a protein matrix. We demonstrate that the accessibility of the pathways and the mechanisms of ligand exchange were modified by mutations. Insertion of bulky aromatic residues in the tunnel corresponding to pathway p1 leads to reduced accessibility to the ligands and a change in mechanism of opening from permanent to transient. We propose that engineering the accessibility of tunnels and the mechanisms of ligand exchange is a powerful strategy for modification of the functional properties of enzymes with buried active sites.

© 2009 Elsevier Ltd. All rights reserved.

**Corresponding author.* E-mail address: jiri@chemi.muni.cz.

Abbreviations used: CC loop, C-terminal cap domain loop (α7/α8 loop); CL, chloride anion; DCL, 2,3-dichloropropane-1-ol; TCP, 1,2,3-trichloropropane; MD, molecular dynamics; NC loop, N-terminal cap domain loop (β6/α4 loop); RAMD, random acceleration molecular dynamics; PDB, Protein Data Bank.

0022-2836/$ - see front matter © 2009 Elsevier Ltd. All rights reserved.

[6]*Molecular and Cellular Modeling Group, EML Research, Schloss-Wolfsbrunnenweg 33, D-69118 Heidelberg, Germany*

Received 11 March 2009; received in revised form 25 June 2009; accepted 29 June 2009
Available online 3 July 2009

Edited by D. Case

Keywords: haloalkane dehalogenase; product release; random acceleration molecular dynamics; tunnel; water exchange

Introduction

Many globular enzymes possess active sites buried in the protein core, and there is growing evidence that the access of substrates to the active site or release of products can be a determinant of their catalytic activity[1–13] and substrate specificity.[1–3,5–8,10,13–21] Mechanisms of ligand exchange between buried active sites and bulk solvent and the effects of mutations on the exchange process are often less well understood than the mechanisms of chemical reactions taking place in the active sites.

The wealth of knowledge that has been acquired about haloalkane dehalogenases (EC 3.8.1.5) in the past two decades makes these enzymes a good model system to study fundamental principles of enzymatic function. Haloalkane dehalogenases belong to the α/β-hydrolase superfamily of enzymes[22] and catalyze hydrolytic dehalogenation of various halogenated aliphatic hydrocarbons to a corresponding alcohol and a halide.[23–25] The reaction is accomplished by a catalytic pentad composed of a nucleophile, a base, a catalytic acid, and two halide-stabilizing residues.[26–29] Two kinetically observable chemical steps are as follows: (i) bimolecular nucleophilic substitution (S_N2) leading to the formation of a halide anion and alkyl-enzyme intermediate and (ii) nucleophilic addition (Ad_N) of a water molecule yielding a tetrahedral intermediate.[30–32] The reaction takes place in a hydrophobic active-site cavity located at the interface of the α/β-hydrolase domain and the helical cap domain.[27,33] The binding of hydrophobic substrates in the buried active site is favorable, shielding the reactive center from bulk water.[33] On the other hand, halide and alcohol products formed during the reaction must be released to allow another substrate molecule to enter the active site for the next catalytic cycle and this process can be rate-limiting.[30,31]

Two tunnels connecting the buried active site with the bulk solvent can be identified in the X-ray crystal structures of DhaA from *Rhodococcus* sp. available in the Protein Data Bank (PDB) structural database: 1CQW, 1BN6, and 1BN7.[27] These tunnels were previously named the main tunnel and the slot tunnel[34,35] and can serve as potential product release pathways. The main tunnel is open in all three structures, whereas the slot tunnel is open only in the structure 1BN6 with five ordered water sites in its mouth opening. A surface representation of structures 1CQW and 1BN7 shows that the slot tunnel is blocked and indicated only by a bulge protruding from the active site. Besides the two tunnels, a significantly deep surface depression near the slot mouth is nearly connected to the active site in all the three structures. The active site is hydrated by three water molecules in 1CQW with iodide bound between the two halide-stabilizing residues. On the other hand, the structure 1BN7 contains an acetate molecule in the active site and the active site of the structure 1BN6 contains an unidentified ligand.[27] Based on available structural information, several intriguing questions regarding the function of the tunnels and the role of solvent for release of products from the buried active site of DhaA can be formulated. Which of the two tunnels is used for release of a halide and an alcohol and for exchange of water molecules between the buried active site and bulk solvent? Are there any other product release pathways and water exchange pathways besides the two tunnels observed in the crystal structures? What is the mechanism for release of products from the buried active site? Could we change accessibility of the pathways by introducing mutations in the tunnels?

Molecular dynamics (MD) simulation is an established approach to study the dynamic behavior of proteins and can be applied for the investigation of release pathways for the two dehalogenation products of 1,2,3-trichloropropane (TCP) conversion in DhaA, that is, chloride anion (CL) and 2,3-dichloropropane-1-ol (DCL). The process of product release from the buried active site of DhaA to bulk solvent may occur on millisecond or longer time scales[31] and, therefore, can be too computationally demanding for classical MD simulations. This problem can be handled by the use of random acceleration molecular dynamics (RAMD) simulations.[14] RAMD is an enhanced sampling technique that

makes ligand release from a buried enzyme active site observable in computationally accessible simulation times.[15] RAMD resembles classical MD simulation except that an additional force is applied to the center of mass of the ligand in a randomly chosen direction. RAMD has been used to investigate substrate and product release pathways in cytochrome P450 enzymes,[14–17] unbinding of retinoic acid from retinoic acid receptor,[36] and release pathways for retinal in rhodopsin.[37]

Here, MD simulations are used to study release of products and exchange of water solvent in the wild-type haloalkane dehalogenase DhaA from *Rhodococcus rhodochrous* NCIMB13064 and eight DhaA mutants. The mutants carry substitutions in the residues lining two tunnels observed in the crystal structures of DhaA. All possible release pathways for two products and exchange pathways for the water molecules (ligands) are identified, and the mechanisms of ligand exchange between the buried active site and bulk solvent are distinguished. The effects of mutations on accessibility of the pathways and the mechanisms of ligand exchange are analyzed and compared with the crystal structures of the wild-type enzyme and three of the mutants.

Results

Construction and characterization of mutants with modified tunnels

Four variants of DhaA (mutants 04, 21, 27, and 31) carrying mutations in the residues lining the tunnels identified by protein X-ray crystallography were obtained by focused directed evolution of DhaA towards improved activity with TCP.[38,39] Here, we complemented this set by another four protein variants (mutants 14, 15, 51, and 52) constructed by site-directed mutagenesis with the aim of introducing additional variation in the main tunnel and the slot tunnel (Table 1 and Fig. 1). Mutant 14 was designed to contain a bulky residue in position 135 located in the slot tunnel. This variant represented a counterpart to mutant 04 carrying a bulky substitution in the main tunnel. Mutant 15 combined bulky residues in the slot tunnel (position 135) and the main tunnel (position 176). Mutants 51 and 52 carried bulky residues in four and five varied positions, respectively (Fig. 1). All constructed mutants were characterized for their activity with TCP using steady-state kinetics, for binding of DCL using inhibition kinetics, and for proper folding by circular dichroism (CD) spectroscopy.

All mutants showed an increase in the rate of TCP conversion except mutant 14, confirming the earlier proposal that a bulky residue at position 176 is essential for enhanced activity with TCP.[40] The highest increase in activity was determined for mutants carrying two aromatic substitutions in the main tunnel. The Michaelis constants determined for the mutants with TCP were similar to those for wild-type DhaA in all variants except mutant 51. An increase in the Michaelis constant for mutant 51 was compensated by the A145F mutation in mutant 52 (Table 1). The same level of K_m of the wild-type enzyme and the mutants corresponds with the fact that the residues targeted by mutagenesis are localized in the access tunnels rather than in the active site. The inhibition of wild-type DhaA and three mutants, 21, 27, and 31, by DCL was studied at a single concentration of TCP and several inhibitor concentrations. The dehalogenase activity of the DhaA variants decreased with increasing concentration of DCL. All tested mutants were inhibited at millimolar concentrations of DCL (K_i ranging from 2.08 to 4.42 mM) similarly to the wild-type enzyme (K_i = 2.50 mM).

Far-UV CD spectra of wild-type DhaA and its mutants exhibited one positive peak at 195 nm and two negative features at 208 and 222 nm, characteristic of α-helical content. Mutants 04, 14, 15, and 31 showed a similar intensity of their CD spectra to wild-type DhaA, confirming that the secondary structure of these enzymes was not significantly affected by the introduced mutations. Mutants 21, 27, 51, and 52 exhibited changes in the intensity of the measured CD spectra compared to wild-type DhaA, which indicated that the inserted mutations had an effect on the specific packing of the residues

Table 1. Mutants and their kinetic parameters for TCP conversion

	Variable residues									
	Slot tunnel			Main tunnel			Slot/main tunnel			
DhaA	135	141	246	145	172	176	245	K_m[a] (mM)	k_{cat}[a] (s^{-1})	k_{cat}/K_m (s^{-1} M^{-1})
WT	I	W	L	A	A	C	V	1.0 (±0.2)	0.04 (±0.01)	40
04	I	W	L	A	A	Y	V	1.7 (±0.1)	0.24 (±0.01)	141
14	F	W	L	A	A	C	V	1.5 (±0.3)	0.05 (±0.02)	33
15	F	W	L	A	A	Y	V	1.8 (±0.2)	0.23 (±0.01)	128
21[b]	L	F	I	A	A	Y	F	1.2 (±0.2)	0.55 (±0.04)	458
27[b]	V	W	I	A	A	Y	F	1.1 (±0.1)	1.02 (±0.06)	927
31[b]	F	W	I	A	A	Y	F	1.2 (±0.1)	1.26 (±0.07)	1050
51	F	W	I	A	F	Y	F	7.1 (±1.1)	0.21 (±0.02)	30
52	F	W	I	F	F	Y	F	1.7 (±0.2)	0.11 (±0.01)	65

[a] Standard deviation is given in parentheses.
[b] From Pavlova *et al.*[39]

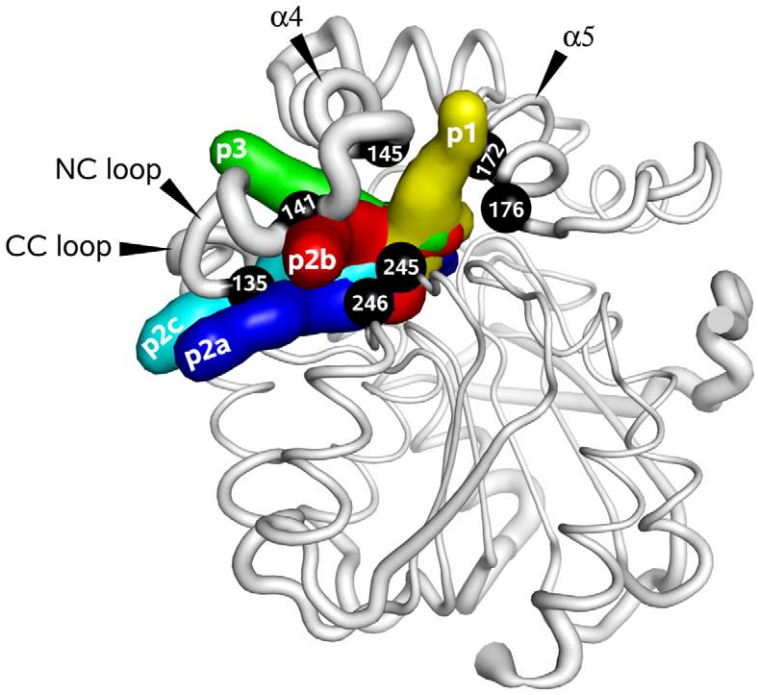

Fig. 1. Spatial location of pathways identified in the wild-type and eight mutants of DhaA from *R. rhodochrous* NCIMB13064. Pathways are represented by the surface and mapped on the crystal structure of DhaA from *Rhodococcus* sp. (PDB ID: 1CQW). The thickness of the ribbon corresponds to the crystallographic *B*-factors. Mutated residues are represented by black balls and labeled by the residue identifier. The color coding of the individual pathways is the same in all figures. p1, the main tunnel; p2a, the slot tunnel. All molecular graphics were created using PyMOL (DeLano Scientific, San Francisco, CA).

in the secondary structure of these enzymes, especially on the overall number of residues contributing to the α-helical content. Although there was an obvious difference in the intensity of the CD spectra among the DhaA variants, the absence of a significant change in the shape of the CD spectra of wild-type DhaA and the mutants suggested that the substitutions did not have a deleterious effect on the folding of the mutants.

Identification of pathways by MD simulations

The structures of the enzyme–product complexes for dehalogenation of TCP were modeled by molecular docking of *R*- and *S*-DCL, respectively, into wild-type DhaA complexed with CL. Both *R*- and *S*-DCL had similar conformations and positions in the active site with respective docked energies of -5.26 and -5.41 kcal mol^{-1} and both formed a hydrogen bond to the D106 side chain and a close contact to the imidazole ring of H272 in the active site. None of the mutated residues in the eight mutants studied overlapped with the binding site of DCL. Therefore, the same initial DCL coordinates were used in all mutants. The complexes were subjected to MD simulations to adjust the conformation of DCL in the active site and the conformations of the mutated residues. During these simulations, DCL preserved its docked orientation, characterized by the strong interactions with the catalytic residues D106 and H272. The overall stability of the complexes was supported by a flattened RMSD around 1.5 Å and a radius of gyration around 17.8 Å for all complexes. The equilibration MD trajectories were investigated for spontaneous release of the products (DCL and CL) and for exchange of water molecules between the buried active site and bulk solvent. In total, one release pathway for CL (p1), no release pathway for DCL, and five pathways for water molecules (p1, p2a, p2b, p2c, and p3) were observed for the DhaA variants. Another set of MD simulations was performed with CL replaced by a water molecule to model the system after release of halide from the active site. The overall stability of the complexes was supported by a flattened RMSD around 1.4 Å and a radius of gyration around 17.8 Å for all complexes. The MD trajectories were investigated for exchange of water molecules and spontaneous release of DCL. Altogether, three pathways were observed for water molecules (p1, p2a, and p2b) with the DhaA variants. No release of DCL was observed in any of the equilibration MD simulations, justifying the use of RAMD simulations to enhance DCL release. RAMD simulations of DCL release in wild-type DhaA and its mutants resulted in five pathways (p1, p2a, p2b, p2c, and p3). All existing pathways and mechanisms for exchange of CL, DCL, and water molecules between the active site and bulk solvent in wild-type DhaA and its mutants are summarized in Table 2 and in Figs. 2 and 3.

Pathway p1

Description of p1

p1 corresponds to the main tunnel identified in the crystal structures of DhaA. p1 is defined mainly by two helices of the cap domain α4 (F144, A/F145, and F149) and α5 (A/F172 and C/Y176) and, to a smaller extent, by the β8/α10 loop (H272) and the β8/α9 loop (V/F245). The main tunnel was permanently open in wild-type DhaA and mutant 14. The tunnel was widened during the passage of DCL, CL, and

Table 2. Occurrence of mechanisms of ligand exchange between the buried active site and bulk solvent in the wild-type (WT) and eight mutants (numbered) of DhaA during classical MD simulations and during RAMD simulations with a random force applied to DCL

Ligand	Pathway	Permanent tunnel	Transient tunnel	Protein matrix
CL	p1	WT	15	—
	p2a	—	—	—
	p2b	—	—	—
	p2c	—	—	—
	p3	—	—	—
DCL	p1	WT, 14	04, 15, 21, 27, 31, 51, 52	—
	p2a	—	WT, 04	—
	p2b	—	27	—
	p2c	—	21	—
	p3	—	WT, 27	—
Water	p1	WT, 14	04, 15, 21, 27, 31, 52	—
	p2a	—	04, 27	—
	p2b	—	WT, 04, 14, 15, 27, 31, 51, 52	—
	p2c	—	04	—
	p3	—	—	21

water molecules. The introduction of one or more aromatic substitutions in p1 caused a change in the opening mechanism from permanent tunnel to the transient tunnel (Fig. 4). Decreased accessibility of the tunnel for the studied ligands was observable already after a single substitution, C176Y in mutant 04, and was further pronounced by cumulatively introduced substitutions V245F, A172F, and A145F in mutants 31, 51, and 52 (Fig. 5d). The accessibility of p1 was controlled by the aromatic residues F144 and F149 in wild-type DhaA; by C176Y, V245F, A172F, and A145F in mutants 04, 15, 21, 27, 31, 51, and 52; by the varying length of the N-terminal part of α4 helix (143-EFA/F-145); by a flexible residue located in the middle of the α5 helix (G171); and by the varying size of the C-terminal part of the α5 helix (C/Y176).

Release of CL through p1

The release of CL was observed only through p1 and only in wild-type DhaA and mutant 15 (Fig. 5a). No release of the CL was observed in the classical MD and RAMD (data not shown) simulations of mutants 04, 14, 21, 27, 31, 51, and 52. The release process in wild-type DhaA started with rapid hydration of the active site by crystallographic water molecules located in p2a, followed by water molecules from bulk water entering the active site through p1 and p2b. The position of the two crystallographic water molecules in p2a was occupied by I135F in mutant 15. Therefore, only p1 and p2b were used by bulk water molecules to access the active site of mutant 15. The water molecules entered the active site and competed with CL for hydrogen-bonding interactions with the halide-stabilizing residues. Eventually, they enabled release of CL by making a hydration shell composed of three to five water molecules that accompanied the CL through the broadly widened p1. The entire release event took about 200 ps counting from the initial destabilization of the CL from the halide-stabilizing residues in both wild-type DhaA and mutant 15. The vacant binding site between the halide-stabilizing residues became occupied by a water molecule. Other water molecules in the active site competed with DCL for a hydrogen-bonding interaction with D106. DCL retained the hydrogen bond to D106 during the entire simulation in mutant 15, whereas in wild-type DhaA, this interaction was broken and DCL interacted with D106 indirectly through a water bridge.

Release of DCL through p1

p1 was the most frequently used pathway for the release of DCL in wild-type DhaA and all the mutants (Fig. 5b). The release process was strongly affected by the hydrogen bond between DCL and the nucleophile D106. This interaction had to be broken by water molecules to enable release of DCL from the active site and entry to the main tunnel. DCL was further attracted to the main tunnel by favorable electrostatic and van der Waals interactions with the catalytic base H272 and occasional hydrogen-bonding interactions with its $N^{\varepsilon 2}$. When the hydrogen bond to H272 was formed, DCL used exclusively pathway p1 for the release. DCL could

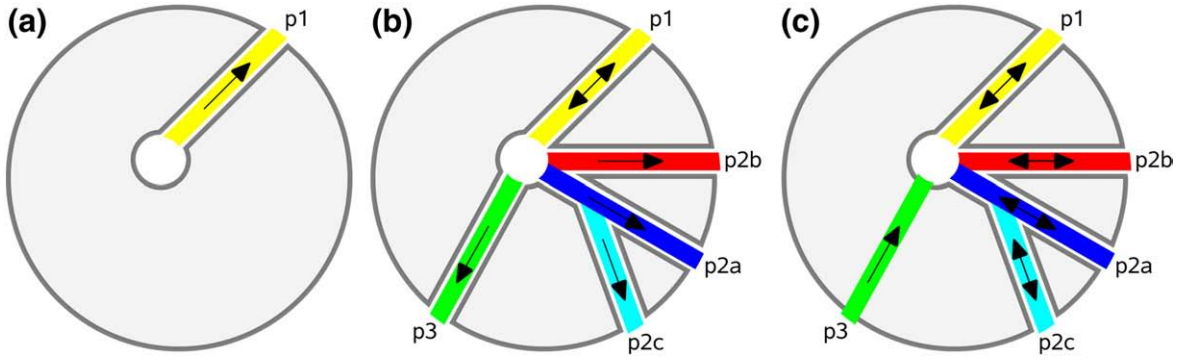

Fig. 2. Schematic representation of pathways for CL (a), DCL (b), and water molecules (c) in the wild-type and eight mutants of DhaA. Arrows indicate direction of passage of ligands through a tunnel or protein matrix (see Fig. 3). p1, the main tunnel; p2a, the slot tunnel.

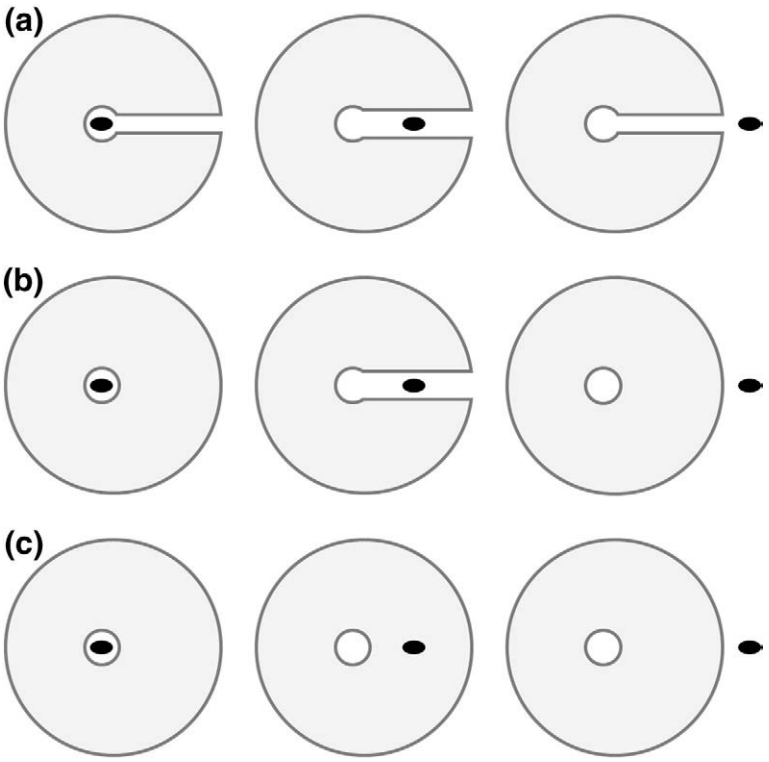

Fig. 3. Schematic representation for three mechanisms of ligand exchange between the buried active site of DhaA and bulk solvent: passage through a permanent tunnel (a), passage through a transient tunnel (b), passage through a protein matrix (c).

also form occasional hydrogen bonds to the thiol group of C176, the hydroxy group of C176Y, and the backbone carbonyl of A172. During the passage, DCL induced opening of p1 by promoting conformational changes in aromatic side chains lining p1. In wild-type DhaA, F144 was occasionally pushed to the bulk solvent to allow release of DCL out of the protein structure. The introduction of bulky aromatic substitutions C176Y and V245F significantly decreased the frequency of release of DCL through p1. The frequency was again increased by introducing additional aromatic substitutions A172F and A145F. The release of DCL from the variants carrying mutations C176Y and V245F required the simultaneous flip of both the aromatic residues followed by a conformational change of F144 to form an open

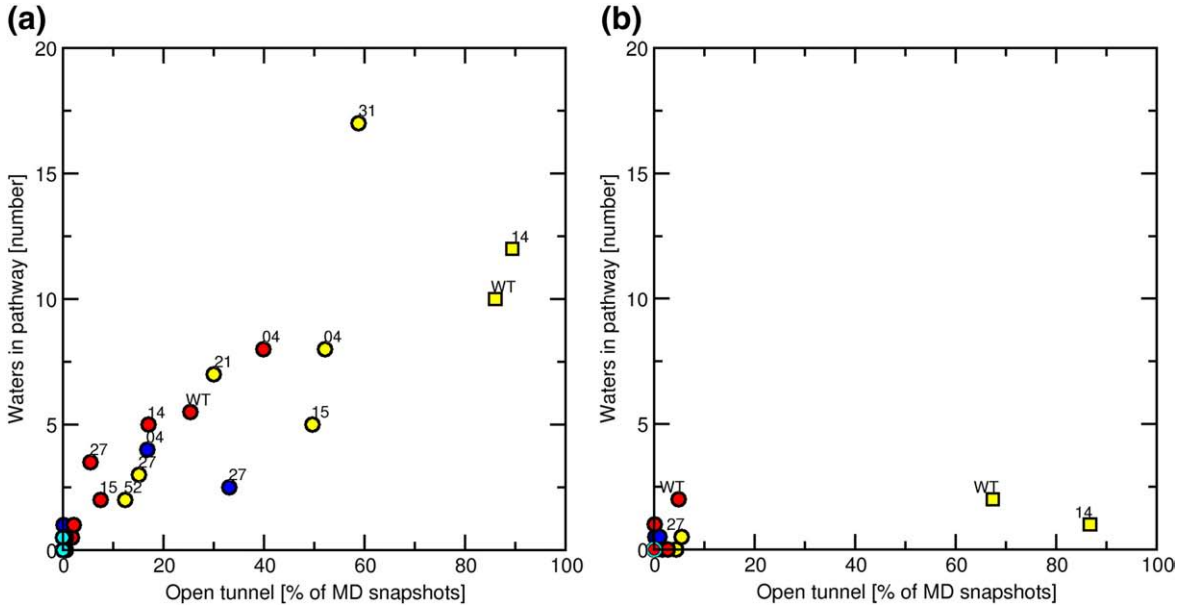

Fig. 4. The effect of mutations on the opening and solvent accessibility of permanent (squares) and transient tunnels (circles) in the wild-type and eight mutants of DhaA with CL (a) and without CL (b) in the active site (see Table 2). Each value represents the average from two independent simulations. Color coding of the pathways: p1, yellow; p2a, blue; p2b, red; p2c, cyan; p3, green.

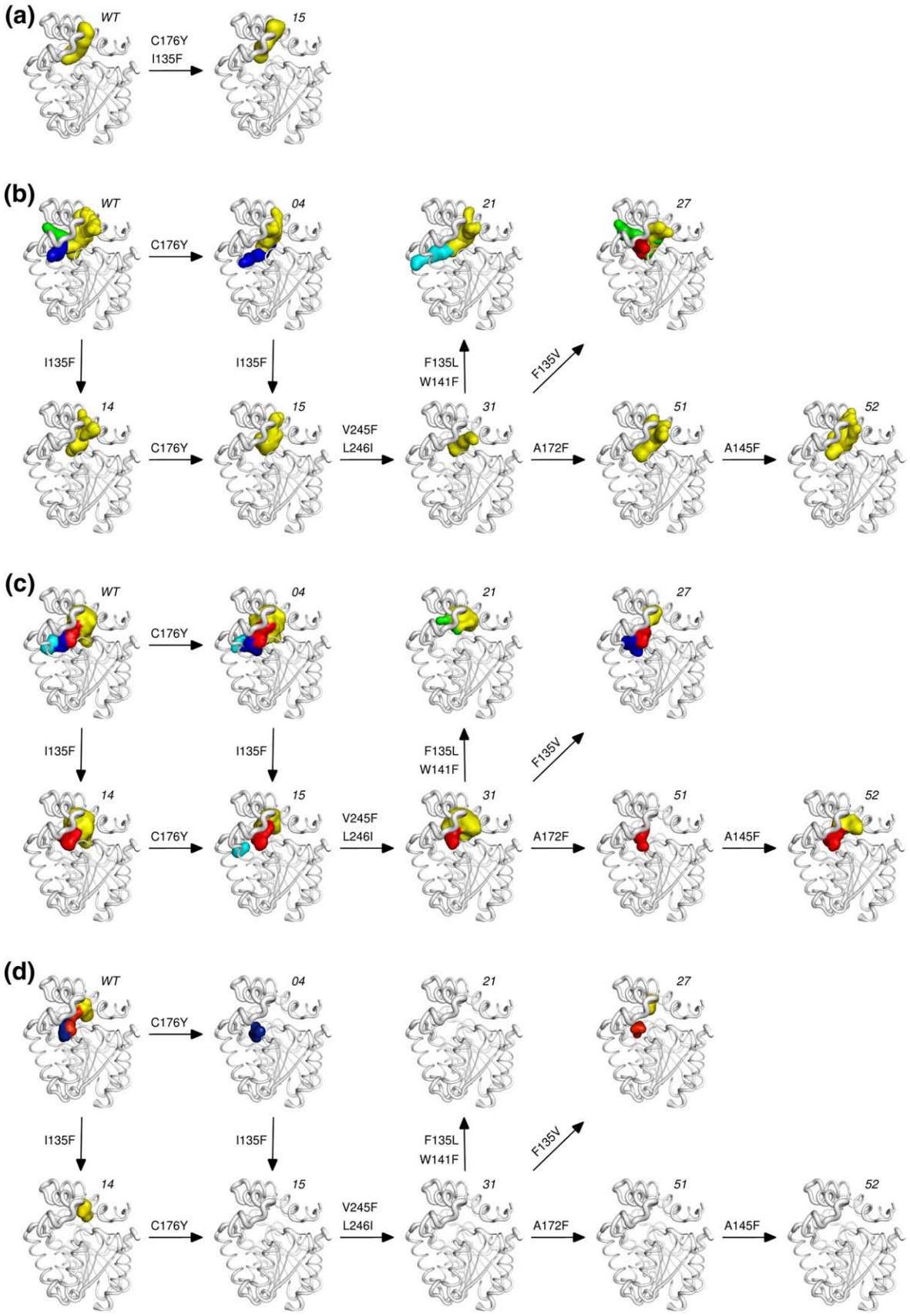

Fig. 5. Effect of mutations on the accessibility of the pathways for CL (a), DCL (b), water molecules with CL in the active site (c), and water molecules without CL in the active site (d). The pathways are depicted by a surface model of selected atoms of ligands in MD or RAMD simulations (see Methods) and mapped onto the crystal structure of DhaA from *Rhodococcus* sp. (PDB ID: 1CQW). DhaA is shown in ribbon; the pathways are color coded: p1, yellow; p2a, blue; p2b, red; p2c, cyan; p3, green.

gate. The release of DCL through p1 in mutant 51 required successive conformational changes in the order A172F, V245F, and C176Y. Additionally, A145F in mutant 52 caused hindrance of DCL release through p1. This steric hindrance was characterized by repeated entry of DCL into the main tunnel and its return back to the active site during the simulations.

Exchange of water molecules through p1

p1 was used by water molecules in all variants, except mutant 51, in the presence of CL in the active site (Fig. 5c). The accessibility of p1 for water molecules was much lower in the absence of CL in the active site (Fig. 5d); aromatic residues introduced into the main tunnel of mutants 04, 15, 21, 27, 31, 51, and 52 prevented the exchange of water molecules through p1 within the 2-ns time scale of the MD simulations.

Pathway p2a

Description of p2a

p2a is equivalent to the slot tunnel observed in the crystal structure 1BN6 of wild-type DhaA. p2a is defined by the β7/α9 loop (L246) and the β6/α4 loop [or N-terminal cap domain loop (NC loop); R133, I135, and W141]. p2a formed an open tunnel only during passage of DCL or water through p2a in the proteins with I135 (wild-type and mutant 04) or V135 (mutant 27). The accessibility of p2a was clearly controlled by residue 135 and by flexibility of the NC loop, the most mobile element of the DhaA structure according to the crystallographic and MD *B*-factors.

Release of DCL through p2a

p2a was accessible for DCL only in wild-type DhaA and mutant 04. The release of DCL through p2a was initiated by the breakage of a hydrogen bond between DCL and D106, immediately followed by formation of a DCL–water–D106 interaction with DCL located in the entry to the slot tunnel. The breakage of the water-bridge interaction resulted in fast passage of DCL towards R133 located at the outer opening of p2a. R133 made strong electrostatic and van der Waals interactions with DCL and additionally formed an unstable salt link with E140 and a stable hydrogen bond with the carbonyl of L246. DCL could form a hydrogen bond with the side chain of R133 when the salt link is naturally broken. Breakage of the salt link was, however, not essential for release of DCL to the bulk solvent.

Exchange of water molecules through p2a

p2a was rarely used by water molecules, and exchange of the solvent occurred only in wild-type DhaA and mutant 04 in both the presence and absence of CL in the active site and in mutant 27 only in the presence of CL in the active site (Fig. 5c and d). A single substitution, I135F, was sufficient to block exchange of water molecules through p2a.

Pathway p2b

Description of p2b

p2b corresponds to the deep surface depression near the slot tunnel opening in the crystal structures of wild-type DhaA. p2b is formed by the β7/α9 loop (V245F and L246I) and the NC loop (R133, I/L/V/F135, and W/F141). p2b formed a tunnel during the passage of DCL or water molecules through the pathway. p2b could be opened simultaneously with p1 and p2a. The accessibility of p2b was controlled by the aromatic residues W/F141 and V245F as well as by the flexibility of the NC loop.

Release of DCL through p2b

Release of DCL through p2b was observed only in mutant 27 carrying the mutation I135V (Fig. 5b). The release process started by breakage of the hydrogen bond between DCL and D106, followed by a DCL–water–D106 interaction and a transient hydrogen bond between DCL and the backbone carbonyl groups of E130 and I132. DCL entered p2b by inducing a simultaneous flip of the V245F and W141 side chains. DCL moved between the two aromatic side chains and established a hydrogen bond to the R133 side chain and the V245F backbone without perturbation of the salt link between R133 and E140 and the hydrogen bond between R133 and L246I. This hydrogen-bonding network hindered the smooth release of DCL to the bulk water.

Exchange of water molecules through p2b

p2b was used by water molecules in all DhaA variants, except mutant 21, in the presence of CL in the active site (Fig. 5c). p2b was the only pathway for exchange of water molecules in mutant 51 and the preferred pathway in mutant 27. p2b was always preferred over p2a, p2c, and p3. The accessibility of p2b for water molecules was significantly decreased in the absence of the CL in the active site. p2b was not used by water molecules in any variant except mutant 27 in MD simulations without CL (Fig. 5d).

Pathway p2c

Description of p2c

p2c was identified as a branch of p2a, which was not indicated by any of the crystal structures of wild-type DhaA. p2c was formed by the NC loop (R133, I135, and W/F141) and the α7/α8 loop [or C-terminal cap domain loop (CC loop); P210 and P212]. p2c formed an open tunnel only in wild-type DhaA and mutant 21 and only in the presence of CL in the active site. The bulkier DCL promoted opening of p2c for a longer time during its release in RAMD simulations. The accessibility of p2c was controlled

by the flexibility of the NC and CC loops and by a β-bridge interaction between P210 and A212 of the CC loop and I135 of the NC loop. The β-bridge must be disrupted to allow exchange of a ligand between bulk solvent and p2c.

Release of DCL through p2c

Release of DCL through p2c was observed only in mutant 21 carrying the unique substitution W141F (Fig. 5b). The release process started by obligatory breakage of the hydrogen bond between DCL and D106, followed by formation of the water bridge DCL–water–D106 positioning DCL near the entrance to p2a and p2c. After breakage of the water bridge, DCL moved along W141F, inducing a flip of its side chain, disrupted the A212–I135L β-bridge interaction, and established a hydrogen bond with the backbone carbonyl group of R133. The arginine showed strong electrostatic and van der Waals attraction for DCL. While maintaining the hydrogen bond to R133, DCL reoriented its carbon chain towards the β-bridge. After release of DCL from R133, DCL moved between the NC loop and the CC loop, causing breakage of the A212–I135L β-bridge interaction followed by release of DCL to bulk water and the immediate reconstruction of the β-bridge. The loss of the hydrogen-bonding interactions between the NC loop and the CC loop during DCL release through p2c was partially compensated for by a hydrogen bond between the residues of the β-bridge and DCL.

Exchange of water molecules through p2c

p2c was rarely used for exchange of water molecules and occurred only in wild-type DhaA and mutant 04 and only in the presence of CL in the active site (Fig. 5c and d). The accessibility of the active site for water molecules through p2c was blocked by I135F, but the β-bridge could be disrupted by water molecules from bulk solvent as observed for the mutant in the presence of CL in the active site.

Pathway p3

Description of p3

p3 was not observable in any crystal structure of wild-type DhaA. p3 was located between helix α4 (F149), the NC loop (W138 and W141), and the CC loop (L209 and I211). p3 was relatively short and straight compared to p2a, p2b, and p2c but was generally unfavorable for accommodation of water molecule or DCL due to steric clashes with the protein structure. p3 formed an open tunnel only upon passage of DCL through the pathway, whereas water migrated through the protein matrix. The open tunnel existed for the shortest period of time (on the order of picoseconds) among the pathways before its disappearance. Water in p3 moved solely through the protein matrix without formation of a tunnel (Fig. 3).

Release of DCL through p3

The release of DCL through p3 occurred in wild-type DhaA and in mutant 27 (Fig. 5b). After obligatory release of DCL from the nucleophile D106, a DCL–water–D106 interaction was established, and DCL was positioned between W141 and F149, whose side chains acted as a gate and flipped to open up the p3 pathway. The immediate release of DCL to the bulk solvent was blocked by the side chain of W138, and DCL was temporarily enclosed in an isolated cavity. DCL eventually pushed W138 into the bulk water and was released out of the protein. After DCL release, W138 made a fast flip to its original conformation to completely block p3.

Exchange of water molecules through p3

p3 served as the exchange pathway for one water molecule in mutant 21 carrying the mutation W141F and CL in the active site (Fig. 5c).

Structural characterization of three mutants with modified tunnels

Protein X-ray crystallography was used to determine the structures of mutants 04, 14, and 15 of DhaA from *R. rhodochrous* NCIMB13064 to atomic resolution (A.S. *et al.*, unpublished results). The mutant structures were compared with the structures of DhaA from *Rhodococcus* sp. available in the structural database.[27] This analysis deciphered the effect of the substitutions located in the main tunnel (mutant 04), the slot tunnel (mutant 14), and both the main and slot tunnels (mutant 15) on the accessibility of the active site and the mechanisms of ligand exchange (Fig. 6).

The main tunnel was open in all crystal structures of DhaA variants carrying the wild-type C176, while the single C176Y substitution blocked this tunnel. This observation was in agreement with MD simulations showing the main tunnel to be mostly closed in mutants 04 and 15, unless it was temporarily opened by a passing ligand. The side chain of Y176 was resolved in two different conformations in the crystal structure of mutant 04. The distance between oxygen atoms of 4-hydroxyphenyl groups of the two conformations is 4.1 Å, and there are most likely two distinct conformational states of this bulky residue at the mobile C-terminus of the α5 helix. Accommodation of the 4-hydroxyphenyl group of Y176 in the place formerly occupied by the thiol group of C176 results in one conformation pointing towards the active site and another placing the aromatic ring close to the carbonyl of A172. This observation is consistent with the gatekeeping function of Y176 and the observation of both conformations of Y176 in the MD simulations.

The opening of the slot tunnel in the structure 1BN6 was due to the presence of different rotamers of I135 and R133 side chains together with 0.8 Å displacement of the backbone of five residues of the NC loop (133-RPIPT-137), compared to structures 1CQW and 1BN7. This is in accordance with the

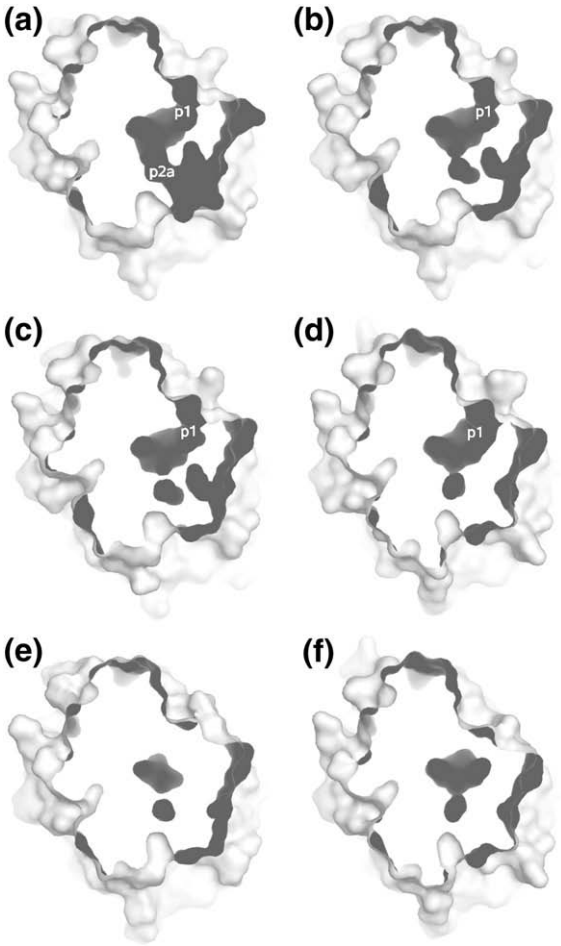

Fig. 6. The crystal structures of DhaA and its mutants ordered by the accessibility of their active sites *via* the main tunnel and the slot tunnel. DhaA from *Rhodococcus* sp. (PDB ID: 1BN6) with the main tunnel and the slot tunnel open (a), DhaA from *Rhodococcus* sp. (PDB ID: 1CQW and 1BN7) and mutant 14 of DhaA from *R. rhodochrous* NCIMB13064 (PDB ID: 3G9X) with the main tunnel open and the slot tunnel closed (b–d), mutants 04 and 15 of DhaA from *R. rhodochrous* NCIMB13064 (PDB ID: 3FBW and 3FWH) with both the main tunnel and the slot tunnel closed (e and f). The protein structures are visualized as a slice through the surface representation with tunnels and cavities colored in dark gray. p1, the main tunnel; p2a, the slot tunnel.

important role of the highly mobile NC loop in controlling the accessibility of the slot tunnel in RAMD simulations of DCL release through the p2a pathway. The displacement of the NC loop in the structure 1BN6 could be due to the presence of an unknown ligand represented by an extensive electron density in the active site and five water molecules located at the mouth of the slot tunnel.[27] On the contrary, the active site of 1CQW contains only water molecules and 1BN7 contains an acetate ion. The slot tunnel in structures 1CQW and 1BN7 was represented only by an isolated cavity containing two water molecules, while no crystallographic water molecules were identified in the region corresponding to the mouth of the slot tunnel.

The NC loop of mutant 04 was resolved in a conformation similar to that in structures 1CQW and 1BN7, resulting in a closed slot tunnel. The introduction of a bulky I135F substitution further reduced accessibility of the slot tunnel of the crystal structures of mutants 14 and 15. The NC loop of mutants 14 and 15 aligned with the corresponding region of 1BN6, suggesting slight displacement of the loop upon introduction of the bulky aromatic side chain. This was in agreement with MD simulations that showed I135 to switch between four different conformations, whereas F135 adopted a single conformation similar to those observed in the crystal structures of mutants 04 and 15. Based on available crystallographic data, we conclude that the slot tunnel belongs to a transient type of tunnel in all the studied proteins, while the main tunnel changes from being a permanent tunnel in the proteins with the wild-type cysteine in position 176 to being a transient tunnel in mutants 04 and 15 carrying tyrosine at position 176.

Discussion

MD simulations identified five pathways for product release and water exchange

Two distinct tunnels, named the main tunnel and the slot tunnel, could be identified in the crystal structures of the haloalkane dehalogenases.[34,35] The simulations conducted with wild-type DhaA confirm the relevance of the main tunnel (pathway p1) and the slot tunnel (pathway 2a) for release of products and exchange of water molecules between the buried active site and the bulk solvent. p1 is observed as the only release pathway for CL. The release of CL was observed only in wild-type DhaA and mutant 15, most probably due to limited time available in the classical MD simulations for the CL to become hydrated. Nevertheless, the proposed role of p1 for CL release is supported by the presence of iodide anions in the wild-type X-ray crystal structure 1CQW.[27] The structure reveals two iodide binding sites: (i) iodide anion positioned between the halide-stabilizing residues N41 and W107 and (ii) iodine covalently attached to the S^{γ} of C176.[27] An imaginary line connecting the two iodide binding sites goes through the p1 pathway. p1 is also the dominant release pathway for DCL and for exchange of water molecules between the active site and bulk solvent. p2a functions as an auxiliary pathway for DCL and water molecules. The release of DCL through the pathway corresponding to p2a was also observed in the recent MD simulations of enzyme–product complexes of the phylogenetically closely related haloalkane dehalogenase LinB.[41]

Besides p1 and p2a, the simulations revealed the additional p2b and p2c for water molecules and p3 for DCL in wild-type DhaA. While p2b can be related to a deep surface depression in the three available crystal structures of DhaA,[27] no indication for p2c or p3 can be found in these structures. DCL passing

through p3 forms a transient tunnel, while water molecules pass directly through the protein matrix of the region p3. MD simulations suggest that p2b and p2c function as auxiliary pathways for water molecules, especially in the presence of charged CL in the active site. Interestingly, p2b is the preferred route for the exchange of water molecules over p2a and is observed in all but one DhaA variant.

It is noteworthy that all the pathways are located along highly mobile secondary-structure elements of the DhaA cap domain comprising the NC loop, the variable N-terminal part of the α4 helix, the breakage point in the α5 helix at G171, and the variable C-terminal part of the α5 helix and the CC loop.[34] The larger backbone fluctuations during the passage of CL, DCL, or water molecules through a pathway compared to the free, unliganded pathway also suggest that the mobility can be further enhanced by interactions with small molecules. Apparently, some of the functionally relevant pathways are not observable in the crystal structures and MD simulations are necessary for their identification.[14–17,36,37] Previous studies on other systems have also shown that flexibility of loops and helices controls accessibility of the active site, for example, in cytochrome P450,[15,17,18,42–50] acetylcholinesterase,[4] gpH1 receptor,[49] and haloalkane dehalogenase LinB.[41] We further demonstrate that all relevant pathways in wild-type DhaA and its mutants can be identified by monitoring of the exchange of solvent between the buried active site and the protein surface.

Solvation of products is essential for their release from buried active site

Specific interactions between the two products, CL and DCL, the protein, and water solvent are essential for release of products from the buried active sites of haloalkane dehalogenases. CL formed during the dehalogenation reaction is strongly bound in between two halide-stabilizing residues, which are present in all currently known haloalkane dehalogenases.[26–29,33,50–55] The halide ion is positioned in between the two halide-stabilizing residues in all crystal structures of haloalkane dehalogenases, with the exception of enzyme–substrate complexes with the halide-binding site occupied by the substrate molecule.[27,33,54] The stabilization of halide ions is weaker in DhaA than in DhlA due to the different chemistry of the halide-stabilizing residues. DhaA possesses tryptophan and asparagine, whereas DhlA has two tryptophans.[53,55] The stronger stabilization of the halide product in DhlA, together with its occluded active site and different location of a catalytic acid, may explain the limitation of the reaction cycle by the halide release.[2,30] In DhaA, halide release is a fast process, showing no effect on overall kinetics.[38] The release of CL from DhaA is clearly triggered by water molecules. The CL bound in the active site induces a strong electrostatic field, which attracts water molecules from the bulk solvent to the active site not only through tunnels p1 and p2a but also through three auxiliary water pathways p2b, p2c, and p3. Water molecules compete with the halide-stabilizing residues for favorable interactions with CL and facilitate the release of CL from the active site. This proposal is in very good agreement with the classical MD simulations of product release from the haloalkane dehalogenase LinB.[41] In DhaA, CL leaves the active site through p1 surrounded by water molecules. The polar residue K175 located at the mouth opening of the main tunnel of DhaA guides solvated CL out of the main tunnel to the surrounding solvent.

Both molecular docking and MD simulations suggest that the DCL, formed during the dehalogenation reaction, makes a hydrogen bond with the nucleophile D106. This interaction could explain inhibition of TCP dehalogenation by DCL product. Disruption of this interaction is assisted by water molecules and represents one of the limiting events of DCL release. Several polar residues located along the release pathways make contacts with DCL during its release. Very important is van der Waals and electrostatic attraction of DCL by H272 in p1. Strong interaction of the alcohol product with the conserved catalytic histidine has been described for the enzyme–DCL complex of LinB[56] as well as for other enzyme–product complexes of this enzyme.[54,57–59] Another important interaction made by DCL, when moving away from the active site *via* p2a, p2b, and p2c, is with the polar R133. R133 controls p2a opening by transient formation of a salt link to E140. Favorable electrostatic and van der Waals interactions are provided by several aromatic side chains in p1, p2b, and p3. Bulky aromatic side chains function as gatekeepers and must undergo conformational change to increase the accessibility of the pathway for bulky DCL. If two or more aromatic side chains form the gate, they change conformation in a simultaneous or consecutive way, depending on their location along the pathway. DCL moves through a pathway taking advantage of temporarily increased local space due to natural protein breathing motions, which may be further enhanced by a DCL molecule. This is in agreement with studies describing the accessibility of pathways that are being controlled locally by (i) hydrogen-bonding and salt link interactions, described for cytochrome P450[14,16,43–45,59–62] and acetylcholinesterase,[63,64] and (ii) aromatic gating, described for cytochrome P450,[14,16,42,43] acetylcholinesterase,[4,64–67] NADH oxidase,[19] horseradish peroxidase,[68,69] and myoglobin.[70]

Mutations change the accessibility of the pathways

The eight mutants of the DhaA haloalkane dehalogenase studied here carry various substitutions in the residues lining the main tunnel and the slot tunnel. The mutations show diverse effects on the accessibility of individual pathways for individual ligands. Four out of five possible pathways (p1, p2a, p2b, and p2c) are accessible for water molecules in wild-type DhaA, whereas one pathway (p3) becomes accessible for water molecules only after

introducing the W141F substitution in mutant 21. Residue 141, together with F149, forms a gate that controls accessibility of p3. The release of DCL through p3 is observed in mutant 27, but not in mutant 21, suggesting that p3 is hardly accessible for bulky alcohol regardless of the residue in position 141. On the other hand, W141F and I135V are required to allow accessibility of p2b and p2c pathways for DCL. I135 is the key residue controlling the access to p2a, p2b, and p2c because its substitution to bulky phenylalanine effectively closes up p2a, p2b, and p2c for DCL and p2a and p2c for water molecules.

The only pathway that could not be completely blocked is p1. This is the main release pathway for DCL and is accessible even after the cumulative introduction of four aromatic substitutions. Introduction of aromatic substitutions in p1 (C176Y, V245F, A172F, and A145F) seems to decrease its accessibility for DCL in the presence of two substitutions but surprisingly seems to restore the accessibility for DCL by the third and fourth substitutions in mutants 51 and 52.

It is noteworthy that many aromatic residues are packed close to each other in the active site (H272, Y273, F152, and F168) and p1 (F144, A145F, F149, A172F, C176Y, and V245F) of mutant 52. We propose that an effective gating is established because product release is not impaired in mutant 52 and the water molecules can enter the occluded active site once CL is formed during the dehalogenation reaction. Such an aromatic gating is a common way by which enzymes with buried active sites control accessibility during the reaction cycle. An interesting example of aromatic gating has been described for acetylcholinesterase.[4,63,65,71] The gate of the main gorge of acetylcholinesterase is formed by four aromatic residues, and their pinching movement,[4,71] together with loop motion[63] and strong dipole moment,[65] is responsible for the enzyme operating near the diffusion-limited rate.

Mutations change the mechanism of ligand exchange

Three different mechanisms for exchange of products and water solvent were observed in the haloalkane dehalogenase DhaA and its mutants: (i) passage through a permanent tunnel, (ii) passage through a transient tunnel, and (iii) passage through a protein matrix. These mechanisms have analogies in other proteins. The exchange of ligands through permanent tunnels has been described for numerous proteins possessing a crystallographically observable tunnel in their structure.[3,4,8,10,17,18,20,34,41,46,72,73] The exchange through the transient tunnels corresponds to exchange through a so-called naturally fluctuating bottleneck,[74] which is a common mechanism to transiently enable access and egress of ligands in and out of the active site in the regions of lower density of protein atoms. This mechanism was previously reported for cytochrome P450,[42,44,47,59] acetylcholinesterase,[66,71] NADH oxidase,[19] T4 lysosyme,[75] and horseradish peroxidase.[69] Passage of the ligands through the protein matrix is a well-documented phenomenon for gas migration in heme proteins.[60,70,72,76,77]

To study the effect of mutations on the mechanism of ligand exchange, we attempted to assign one of three mechanisms to every ligand exchange observed in our molecular dynamic simulations. By comparing the mechanisms of the wild-type enzyme with its mutants, we demonstrated that substitutions introduced into the tunnels changed not only the accessibility of the individual pathways (described in the previous section) but also the mechanism of ligand exchange in the case of the p1 pathway. This pathway follows the permanent tunnel in the wild-type enzyme. The crystal structures of the mutants show that a single aromatic substitution in the tunnel results in its closure. However, MD reveals that ligands can pass through the p1 pathway even in the mutants with four aromatic substitutions. This is possible due to ligand-induced changes in the protein structure that cause the pathway to open up transiently to allow release of products. The opening of p1 can also be induced by water molecules entering the active site through p1 due to strong electrostatic attraction by CL. This solvation of the active site through the transiently opened tunnel is observed even in mutant 52 with the most occluded active site. The substitutions for aromatic residues in p1 clearly changed the mechanism for ligand exchange from the passage through a permanent tunnel to the passage through a transient tunnel.

Concluding remarks

We conclude from our study of the wild-type haloalkane dehalogenase DhaA from *R. rhodochrous* NCIMB13064 and its eight mutants that the ligands can be exchanged between the buried active site and the bulk solvent by five different pathways, denoted p1, p2a, p2b, p2c, and p3, and by three mechanisms, namely, passage through a permanent tunnel, passage through a transient tunnel, and passage through a protein matrix. Two out of the five pathways (p1 and p2a) are observable in the crystal structures, while all the three other pathways were identified by MD simulations.

The release of CL proceeds exclusively *via* pathway p1 and is accompanied by solvation of the negatively charged ion by water molecules, breakage of attractive interactions with the halide-stabilizing residues N41 and W107, and attraction by the polar K175, positioned at the tunnel opening. The release of DCL proceeds *via* all five pathways and requires the initial breakage of the hydrogen bonds between the product molecule, the nucleophile D106, and the catalytic histidine H272. Release of DCL *via* ligand-induced pathways is enabled by the high mobility of the protein backbone and by progressive rotations of the protein side chains leading to formation of transient tunnels. Point mutations systematically introduced into the p1 and p2a tunnels, identified

in the crystal structures, modulate the accessibility of the individual pathways and lead to a changed mechanism of ligand passage in p1. We propose that the accessibility and mechanisms of ligand passage in enzymes with buried active sites can be modulated by mutations introduced into the exchange pathways. These mutations may lead to pronounced effects on enzymatic activities and substrate specificities.

Materials and Methods

Mutagenesis and DNA sequencing

Established methods were employed for the preparation of plasmid DNA, digestion of plasmid and PCR-amplified DNA fragments with restriction endonucleases, ligation, agarose gel electrophoresis, and transformation of *Escherichia coli* cells.[78] The construction of the recombinant genes *dhaA04His*, *dhaA21His*, *dhaA27His*, and *dhaA31His* was described by Pavlova *et al.*[39] The mutant recombinant genes *dhaA14His* and *dhaA15His* were obtained using the QuikChange Site-Directed Mutagenesis Kit (Stratagene, La Jolla, CA) according to the manufacturer's instructions. Plasmids pUC18::*dhaAHis* and pAQN::*dhaA04His* were used as templates.[79] The recombinant gene *dhaA14His* was afterwards recloned into the expression vector pAQN. The mutant genes *dhaA51His* and *dhaA52His* were constructed by site-directed mutagenesis using the principle of inverted PCR that was carried out according to the protocol provided with Phusion polymerase (Finnzymes, Espoo, Finland). pAQN::*dhaA31His* and pAQN::*dhaA51-His* were used as templates. The nucleotide sequences of all mutants were determined by the dideoxy chain termination method using an automated DNA sequencer, ABI PRISM 310 genetic analyzer (Applied Biosystems, Foster City, CA).

Protein expression and purification

The expression and purification of wild-type DhaA and mutants 04, 21, 27, and 31 were described by Pavlova *et al.*[39] The recombinant plasmids pAQN::*dhaA14His*, pAQN::*dhaA15His*, pAQN::*dhaA51His*, and pAQN::*dhaA52His* were transformed to *E. coli* BL21 cells. Fresh transformants were used to inoculate 2 L of Luria–Bertani medium (Sigma-Aldrich, St. Louis, MO) with ampicillin (100 μg/mL) and cultivated at 37 °C to an optical density of 0.5 at 600 nm. Protein expression was induced by addition of isopropyl-D-1-thiogalactopyranoside to a final concentration of 0.5 mM in Luria–Bertani medium. Cells were harvested by centrifugation at 8000*g* for 10 min after 4 h of cultivation at 30 °C. During harvesting, cells were washed and then resuspended in 20 mM KH_2PO_4 buffer (pH 7.5). Harvested cells were kept at −65 °C. Defrosted cell suspensions were disrupted by sonication with Soniprep 150 (Sanyo Gallenkamp, Loughborough, UK) or ultrasonic processor Hielscher UP200S (Hielscher Ultrasonics, Teltow, Germany), and the lysates were centrifuged at 21,000*g* for 1 h. The collected cell-free extracts were purified using FPLC Akta (Amersham Pharmacia Biotech, USA) and HiTrap Chelating column with affinity resin (Amersham Biosciences, Freiburg, Germany) charged with Ni^{2+} and equilibrated with purification buffer (pH 7.5) composed of 16.4 mM K_2HPO_4, 3.6 mM KH_2PO_4, and 0.5 M NaCl containing 10 mM imidazole. Unbound and weakly bound fractions were washed out with the purification buffer containing 50 mM imidazole. Histidine-tagged proteins were eluted with the purification buffer containing 300 mM imidazole. Purified proteins were dialyzed against 50 mM phosphate buffer (pH 7.5) composed of 41 mM K_2HPO_4 and 9 mM KH_2PO_4. Protein concentrations were determined by the method of Bradford (Sigma-Aldrich).

CD spectroscopy

CD spectra were recorded at room temperature (22 °C) using a spectrometer Jasco J-810 (Jasco, Tokyo, Japan). Data were collected from 190 to 260 nm at 100 nm/min, 1 s response time, and 2 nm bandwidth using a 0.1-cm quartz cuvette. Averages of 10 individual scans were corrected for absorbance caused by the buffer and expressed in terms of the mean residue ellipticity (Θ_{MRE}). Secondary-structure content was calculated from the CD spectra using K2D and Self-Consistent methods[80,81] implemented in the program DICROPROT.[82]

Enzyme kinetics

Steady-state kinetic constants K_m and k_{cat} for the conversion of TCP by wild-type DhaA and mutants 04, 14, 15, 21, 27, 31, 51, and 52 were assayed with TCP using the initial velocity measurements described previously.[7] The substrate concentration was assayed by a gas chromatography system equipped with a flame ionization detector Trace GC 2000 (Thermo Finnigan, San Jose, CA) and a DB-FFAP capillary column 30 m × 0.25 mm × 0.25 mm (J&W Scientific, Folsom, CA). The method described previously by Iwasaki *et al.* was used for determination of the product concentration.[83] The K_m and k_{cat} constants were calculated using the computer program Origin 6.1 (OriginLab, Northampton, MA).

Inhibition kinetics

Inhibition constants of wild-type DhaA and mutants 21, 27, and 31 for DCL were determined by monitoring the initial rates of TCP conversion at various DCL concentrations by the spectrophotometric method of Iwasaki. The substrate concentration was constant (1.4 mM), and the inhibitor concentrations varied between 1.4 and 35.0 mM. The velocity of the reaction without the inhibitor was measured as a negative control. Reactions were performed in duplicates. Halide concentrations were determined at several times (10, 20, 30, and 40 min) in order to obtain at least three data points in the initial phase of conversion. Initial substrate and inhibitor concentrations were determined before reaction initiation by gas chromatograph equipped with a flame ionization detector Trace GC 2000 (Thermo Finnigan) and a DB-FFAP capillary column 30 m × 0.25 mm × 0.25 mm (J&W Scientific). Steady-state inhibition constant K_i of DhaA variants for TCP conversion were determined by the initial rate of enzymatic activity using the program ORIGIN 6.1 (OriginLab).

Preparation of structures for molecular modeling

The crystal structure of 1CQW was truncated by five residues at the C-terminus and modified with three substitutions V172A, I209L, and A292G (numbered according to the *dhaA* gene, which differs from the numbering in the

structure by 11 amino acids) to mimic the structure of DhaA from *R. rhodochrous* NCIMB13064 (wild-type DhaA) used in experiments. Mutants 04, 14, 15, 21, 27, 31, 51, and 52 were prepared by the mutagenesis wizard of PyMOL 0.97,[84] selecting the most frequently occurring rotamer that had no steric overlap with the neighboring protein atoms. A three-dimensional model of DCL was built in PyMOL and geometry optimized by the AM1 method of MOPAC 2000 using the following keywords: SCFCRT = 1D-12, EF, GNORM = 0.0001, STEP = 15, POINTS = 12, LET, and PRECISE.[85] The optimized structure was refined by energy minimization using GAUSSIAN 94 employing the Hartree–Fock method and 6-31G* basis set.[86] Partial atomic charges were fitted to reproduce the electrostatic potential calculated with GAUSSIAN using the RESP module of AMBER 8.[87]

Molecular docking

Docking of DCL to wild-type DhaA, considering both *R*- and *S*-DCL, was performed using AUTODOCK 3.05.[88] Rotatable bonds were assigned to DCL using the Autotors module of AUTODOCK. All crystallographic water molecules were removed, the main tunnel iodide was removed, and the active-site iodide was replaced by a CL. Polar hydrogens were added to wild-type DhaA using WHATIF 5,[89] and solvation parameters were added using the Autogrid module of AUTODOCK. A grid box of $81 \times 81 \times 81$ points in x, y, and z dimensions was used with a grid spacing of 0.25 Å. The grid was centered on the C^{γ} of H272 to ensure that the entire active site, the open main tunnel, and the closed slot tunnel were encompassed by the box. The electrostatic map and atomic interaction maps for all atom types of DCL, that is, carbon, oxygen, chlorine, and hydrogen, were calculated using AUTOGRID. Fifty independent docking calculations were performed for *R*- and *S*-DCL using the AUTODOCK module of AUTODOCK using a Lamarckian genetic algorithm for global and a Solis&Wets algorithm for local search with an initial population size of 50 and default AUTODOCK 3.05 settings for elitism and crossover. A maximum of 27,000 generations or 1,500,000 energy evaluations were performed. The resulting conformations were clustered with a tolerance of 0.5 Å. The lowest-energy representations of the highest-populated clusters of *R*- and *S*-DCL in wild-type DhaA were selected as starting conformations for subsequent MD simulations of wild-type DhaA and its mutants.

Classical MD simulations

The AMBER94 force field[90] was used. CL was approximated by the IM atom type of the 1994 Cornell force field[90] and was assigned a charge of −1e. Alternatively, the CL was replaced by one water molecule to approximate the situation with the CL absent. All crystallographic water molecules not overlapping with the docked DCL were added to the complexes. Nonpolar hydrogens were added to the protein using the Leap module of AMBER 8. Seventeen sodium cations were added with Leap to ensure a neutral net charge of the system. Finally, the complexes were immersed in a rectangular box of TIP3P[91] water molecules with a minimum wall thickness of 10 Å using Leap and subjected to an equilibration protocol using the Sander module of AMBER. The equilibrations consisted of the following steps: (i) 300 steps of steepest descent energy minimization of all non-crystallographic atoms, that is, all hydrogens on protein, water, and DCL atoms; (ii) 20 ps periodic boundary condition MD of water, sodium cations, and DCL at constant temperature of 300 K (using the weak-coupling algorithm)[92] and constant pressure of 1 atm (with isotropic position scaling) with the rest of the system harmonically restrained with a 500 kcal mol^{-1} $Å^{-2}$ force constant; (iii) four consecutive steepest descent energy minimizations of 300 steps each with a decreasing restraint on the protein backbone with a force constant of 500, 125, 5, and 0 kcal mol^{-1} $Å^{-2}$ respectively; (iv) unrestrained MD using the same parameters as those for the 20 ps of MD but raising the temperature from 0 to 300 K during the initial 200 ps. The trajectories were propagated for 2.0 to 2.8 ns to ensure acquisition of well-equilibrated and stable systems. A time step of 2 fs was used with application of SHAKE algorithm[93] to bonds involving hydrogens and a particle mesh Ewald treatment of Coulombic interactions. The cutoff distance for the nonbonded interactions was 10 Å. Snapshots were gathered every 0.5 ps.

Random acceleration MD simulations

RAMD simulation[14] resembles classical MD simulation except that an additional force is applied to the center of mass of the ligand in a randomly chosen direction. After a user-defined number of time steps, the distance traveled by the ligand is compared to a threshold parameter. If the ligand does not reach the threshold distance, a new, randomly chosen direction is given to the force on its center of mass; otherwise, the force direction is maintained. The process is iterated until the ligand has been released into the bulk solvent. RAMD simulations were carried out using the AMBER 8 software package†.

RAMD was performed on DCL in the CL-free complexes for wild-type DhaA and its mutants. First, the proper setting of the RAMD parameters was tested on wild-type DhaA complexed with *R*- and *S*-DCL, respectively. A random acceleration of 0.25, 0.20, 0.15, 0.1, 0.09, 0.08, 0.07, 0.06, 0.05, 0.04, 0.03, 0.02, and 0.01 kcal $Å^{-1}$ g^{-1} applied to the center of mass of DCL; a number of time steps (10, 20, 40, and 80); and a threshold distance of 0.001, 0.002, 0.004, and 0.008 Å were tested. RAMD simulations were performed with various combinations of the values of the three parameters. Three different snapshots of the MD simulations from a well-equilibrated region were used as starting structures for RAMD simulations, resulting in six RAMD trajectories for each combination of the parameters considering *R*- and *S*-DCL together. The maximum duration of RAMD simulations was set to 1 ns. If DCL left the protein for the bulk water and the distance between center of mass of D106 and DCL exceeded 30 Å, the simulations were halted. RAMD simulations were selected for detailed analysis when the parameters used resulted in the release of *R*- or *S*-DCL within 1 ns in at least 4 out of 6 simulations and lasted for at least 20 ps. The final settings were 0.04 and 0.05 kcal $Å^{-1}$ g^{-1} for the random acceleration, 10 for the number of time steps, and 0.002 and 0.004 Å for the threshold distance, resulting in a total of 24 RAMD simulations of wild-type DhaA. The parameters derived from RAMD simulations of wild-type DhaA were adopted for the mutants. RAMD simulations of the mutants were also performed on *R*- and *S*-DCL, but only the final MD snapshot was used. Altogether, 62 RAMD trajectories of DhaA mutants were recorded. No difference in the preferential release through different pathways or in the mechanism of the release was obvious for the *R*- and *S*-

† The RAMD patch is available at http://projects.villa-bosch.de/mcm/software/amber

enantiomers of DCL. Therefore, *R*-DCL and *S*-DCL were further considered to provide variability in the MD trajectories only. RAMD simulations were also performed in the presence of CL (data not shown).

Analysis of MD simulations

The stability of the trajectories was assessed by RMSD and radius of gyration using the Ptraj and Carnal modules of AMBER. Stable parts of the MD simulations were decided visually by plotting RMSD *versus* time. The stability of the secondary elements was calculated in PyMOL for each snapshot of a trajectory using the DSSP method.[94] *B*-factors and geometrical parameters (distances, angles, and dihedrals) were measured using Ptraj. Hydrogen bonds were identified using <2.76 Å and >120° for the distance and angle thresholds, respectively. Distances between the center of mass of the two hydrogen atoms, $H^{\varepsilon 1}$ of W107 and $H^{\delta 22}$ of N41, and CL and between the center of mass of D106 and DCL were measured with Ptraj to identify regions of long residence time for CL or DCL during release from the active site to the bulk water. Residues within 7 Å of the center of mass of DCL along the trajectories were assumed to constitute the release pathways. Seven angstroms ensured that all first shell residues were included. Water molecules that resided in the protein interior or entered the protein during MD and RAMD simulations were identified as those located at a distance less than 8 Å from any atom of D106 in at least one snapshot using Carnal. The selected pathway residues and the internal water molecules aided analysis of important events using VMD 1.8.5[95] and PyMOL where especially behavior of the pathway residues and the internal water molecules were monitored. Release pathways for CL in MD and DCL in RAMD simulations were visualized by PyMOL as a surface representation of CL or all positions of a central carbon of DCL. The surface representations of all release pathways for CL and DCL from all RAMD simulations were superimposed onto the crystal structures of DhaA (PDB codes 1CQW and 1BN6) and clustered by visual inspection according to overlap between the surface representations of the pathways and the contribution of the same secondary-structure elements. Clusters were annotated by a number, and branching clusters were further distinguished by a letter. Water pathways were identified in MD simulations by superimposing all positions of oxygen atoms of all internal water molecules onto the crystal structures of DhaA in PyMOL. Opening and closing of tunnels connecting the active site to the bulk solvent and their inducibility by CL, DCL, and water were visualized by PyMOL as a slice through the solvent-accessible surface representation (with a probe radius of 1.4 Å) of the protein with 5- and 1-ps windows for MD and RAMD simulations, respectively. Tunnels were classified as closed or open according to whether the solvent-accessible surface shows the active site isolated from (closed) or connected to (open) the bulk solvent.

Interaction energies

All snapshots were extracted from the selected RAMD trajectories. All water molecules were removed and the structures were adjusted by 150 steps of steepest descent energy minimization with the implicit generalized Born solvation model II[96] using Sander. The van der Waals and electrostatic interaction energies between DCL and every protein residue were calculated for each of the energy-minimized structures using the Anal module of AMBER.

Accession numbers

Coordinates and structure factors of the X-ray crystal structures of the haloalkane dehalogenase DhaA mutants have been deposited in the PDB with accession numbers 3FBW (mutant 04; C176Y), 3G9X (mutant 14; I135F), and 3FWH (mutant 15; I135F+C176Y).

Acknowledgements

We acknowledge financial support from the Ministry of Education of the Czech Republic (LC06010 to M.P., MSM0021622412 to Martin Klvana, and MSM0021622413 to Z.P.), the Grant Agency of the Czech Republic (201/07/0927 to Jiri Damborsky and 203/08/0114 to R.C.), the Grant Agency of the Czech Academy of Sciences (IAA401630901 to Jiri Damborsky), the North Atlantic Treaty Organization (EST.CLG.980504—NATO Linkage Grant to R.W. and Jiri Damborsky), and the Klaus Tschira Foundation (R.W.). We acknowledge the Supercomputing Center Brno for computational resources.

Supplementary Data

Supplementary data associated with this article can be found, in the online version, at doi:10.1016/j.jmb.2009.06.076

References

1. Zamocky, M., Herzog, C., Nykyri, L. M. & Koller, F. (1995). Site-directed mutagenesis of the lower parts of the major substrate channel of yeast catalase A leads to highly increased peroxidatic activity. *FEBS Lett.* **367**, 241–245.
2. Pikkemaat, M. G., Ridder, I. S., Rozeboom, H. J., Kalk, K. H., Dijkstra, B. W. & Janssen, D. B. (1999). Crystallographic and kinetic evidence of a collision complex formed during halide import in haloalkane dehalogenase. *Biochemistry*, **38**, 12052–12061.
3. Sevinc, M. S., Mate, M. J., Switala, J., Fita, I. & Loewen, P. C. (1999). Role of the lateral channel in catalase HPII of *Escherichia coli*. *Protein Sci.* **8**, 490–498.
4. Tara, S., Helms, V., Straatsma, T. P. & McCammon, J. A. (1999). Molecular dynamics of mouse acetylcholinesterase complexed with huperzine A. *Biopolymers*, **50**, 347–359.
5. Schmitt, J., Brocca, S., Schmid, R. D. & Pleiss, J. (2002). Blocking the tunnel: engineering of *Candida rugosa* lipase mutants with short chain length specificity. *Protein Eng.* **15**, 595–601.
6. Scott, E. E., He, Y. Q. & Halpert, J. R. (2002). Substrate routes to the buried active site may vary among cytochromes P450: mutagenesis of the F–G region in P450 2b1. *Chem. Res. Toxicol.* **15**, 1407–1413.
7. Chaloupkova, R., Sykorova, J., Prokop, Z., Jesenska, A., Monincova, M., Pavlova, M. *et al.* (2003). Modification of activity and specificity of haloalkane dehalogenase from *Sphingomonas paucimobilis* UT26 by engineering of its entrance tunnel. *J. Biol. Chem.* **278**, 52622–52628.

8. Chelikani, P., Carpena, X., Fita, I. & Loewen, P. C. (2003). An electrical potential in the access channel of catalases enhances catalysis. *J. Biol. Chem.* **278**, 31290–31296.
9. Fishman, A., Tao, Y., Bentley, W. E. & Wood, T. K. (2004). Protein engineering of toluene 4-monooxygenase of *Pseudomonas mendocina* KR1 for synthesizing 4-nitrocatechol from nitrobenzene. *Biotechnol. Bioeng.* **87**, 779–790.
10. Jakopitsch, C., Droghetti, E., Schmuckenschlager, F., Furtmüller, P. G., Smulevich, G. & Obinger, C. (2005). Role of the main access channel of catalase–peroxidase in catalysis. *J. Biol. Chem.* **280**, 42411–42422.
11. Zhou, Y., Zheng, Q., Li, Z., Zhang, Y., Sun, M., Sun, C. *et al.* (2006). On the human CYP2C9∗13 variant activity reduction: a molecular dynamics simulation and docking study. *Biochimie*, **88**, 1457–1465.
12. Kotik, M., Stepanek, V., Kyslik, P. & Maresova, H. (2007). Cloning of an epoxide hydrolase-encoding gene from *Aspergillus niger* M200, overexpression in *E. coli*, and modification of activity and enantioselectivity of the enzyme by protein engineering. *J. Biotechnol.* **132**, 8–15.
13. Silberstein, M., Damborsky, J. & Vajda, S. (2007). Exploring the binding sites of the haloalkane dehalogenase DhlA from *Xanthobacter autotrophicus* GJ10. *Biochemistry*, **46**, 9239–9249.
14. Lüdemann, S. K., Lounnas, V. & Wade, R. C. (2000). How do substrates enter and products exit the buried active site of cytochrome P450cam? 1. Random expulsion molecular dynamics investigation of ligand access channels and mechanisms. *J. Mol. Biol.* **303**, 797–811.
15. Schleinkofer, K., Sudarko, Winn, P. J., Lüdemann, S. K. & Wade, R. C. (2005). Do mammalian cytochrome P450s show multiple ligand access pathways and ligand channeling? *EMBO Rep.* **6**, 584–589.
16. Winn, P. J., Lüdemann, S. K., Gauges, R., Lounnas, V. & Wade, R. C. (2002). Comparison of the dynamics of substrate access channels in three cytochrome P450s reveals different opening mechanisms and a novel functional role for a buried arginine. *Proc. Natl Acad. Sci. USA*, **99**, 5361–5366.
17. Wade, R. C., Winn, P. J., Schlichting, I. & Sudarko (2004). A survey of active site access channels in cytochromes P450. *J. Inorg. Biochem.* **98**, 1175–1182.
18. Cojocaru, V., Winn, P. J. & Wade, R. C. (2007). The ins and outs of cytochrome P450s. *Biochim. Biophys. Acta*, **1770**, 390–401.
19. Hritz, J., Zoldak, G. & Sedlak, E. (2006). Cofactor assisted gating mechanism in the active site of NADH oxidase from *Thermus thermophilus*. *Proteins*, **64**, 465–476.
20. Wen, Z., Baudry, J., Berenbaum, M. R. & Schuler, M. A. (2005). Ile115Leu mutation in the SRS1 region of an insect cytochrome P450 (CYP6B1) compromises substrate turnover via changes in a predicted product release channel. *Protein Eng. Des. Sel.* **18**, 191–199.
21. Huang, X. & Raushel, F. M. (2000). An engineered blockage within the ammonia tunnel of carbamoyl phosphate synthetase prevents the use of glutamine as a substrate but not ammonia. *Biochemistry*, **39**, 3240–3247.
22. Ollis, D. L., Cheah, E., Cygler, M., Dijkstra, B., Frolow, F., Franken, S. M. *et al.* (1992). The α/β hydrolase fold. *Protein Eng.* **5**, 197–211.
23. Janssen, D. B., Pries, F., van der Ploeg, J., Kazemier, B., Terpstra, P. & Witholt, B. (1989). Cloning of 1,2-dichloroethane degradation genes of *Xanthobacter autotrophicus* GJ10 and expression and sequencing of the *dhlA* gene. *J. Bacteriol.* **171**, 6791–6799.
24. Nagata, Y., Imai, R., Sakai, A., Fukuda, M., Yano, K. & Takagi, M. (1993). Isolation and characterization of tn5-induced mutants of *Pseudomonas paucimobilis* UT26 defective in gamma-hexachlorocyclohexane dehydrochlorinase (LinA). *Biosci. Biotechnol. Biochem.* **57**, 703–709.
25. Curragh, H., Flynn, O., Larkin, M. J., Stafford, T. M., Hamilton, J. T. & Harper, D. B. (1994). Haloalkane degradation and assimilation by *Rhodococcus rhodochrous* NCIMB13064. *Microbiology*, **140**, 1433–1442.
26. Krooshof, G. H., Kwant, E. M., Damborsky, J., Koca, J. & Janssen, D. B. (1997). Repositioning the catalytic triad aspartic acid of haloalkane dehalogenase: effects on stability, kinetics, and structure. *Biochemistry*, **36**, 9571–9580.
27. Newman, J., Peat, T. S., Richard, R., Kan, L., Swanson, P. E., Affholter, J. A. *et al.* (1999). Haloalkane dehalogenases: structure of a *Rhodococcus* enzyme. *Biochemistry*, **38**, 16105–16114.
28. Janssen, D. B. (2004). Evolving haloalkane dehalogenases. *Curr. Opin. Chem. Biol.* **8**, 150–159.
29. Chovancova, E., Kosinski, J., Bujnicki, J. M. & Damborsky, J. (2007). Phylogenetic analysis of haloalkane dehalogenases. *Proteins*, **67**, 305–316.
30. Schanstra, J. P., Kingma, J. & Janssen, D. B. (1996). Specificity and kinetics of haloalkane dehalogenase. *J. Biol. Chem.* **271**, 14747–14753.
31. Bosma, T., Pikkemaat, M. G., Kingma, J., Dijk, J. & Janssen, D. B. (2003). Steady-state and pre-steady-state kinetic analysis of halopropane conversion by a *Rhodococcus* haloalkane dehalogenase. *Biochemistry*, **42**, 8047–8053.
32. Prokop, Z., Monincova, M., Chaloupkova, R., Klvana, M., Nagata, Y., Janssen, D. B. & Damborský, J. (2003). Catalytic mechanism of the haloalkane dehalogenase LinB from *Sphingomonas paucimobilis* UT26. *J. Biol. Chem.* **278**, 45094–45100.
33. Verschueren, K. H., Seljee, F., Rozeboom, H. J., Kalk, K. H. & Dijkstra, B. W. (1993). Crystallographic analysis of the catalytic mechanism of haloalkane dehalogenase. *Nature*, **363**, 693–698.
34. Otyepka, M. & Damborsky, J. (2002). Functionally relevant motions of haloalkane dehalogenases occur in the specificity-modulating cap domains. *Protein Sci.* **11**, 1206–1217.
35. Petrek, M., Otyepka, M., Banas, P., Kosinova, P., Koca, J. & Damborsky, J. (2006). CAVER: a new tool to explore routes from protein clefts, pockets and cavities. *BMC Bioinformatics*, **7**, 316.
36. Carlsson, P., Burendahl, S. & Nilsson, L. (2006). Unbinding of retinoic acid from the retinoic acid receptor by random expulsion molecular dynamics. *Biophys. J.* **91**, 3151–3161.
37. Wang, T. & Duan, Y. (2007). Chromophore channeling in the G-protein coupled receptor rhodopsin. *J. Am. Chem. Soc.* **129**, 6970–6971.
38. Bosma, T., Damborsky, J., Stucki, G. & Janssen, D. B. (2002). Biodegradation of 1,2,3-trichloropropane through directed evolution and heterologous expression of a haloalkane dehalogenase gene. *Appl. Environ. Microbiol.* **68**, 3582–3587.
39. Pavlova, M., Klvana, M., Prokop, Z., Chaloupkova, R., Banas, P., Otyepka, M. *et al.* (2009). Redesigning dehalogenase access tunnels as a strategy for degrading an anthropogenic substrate. *Nat. Chem. Biol.* (in press). doi:10.1038/nchembio.205.

40. Banas, P., Otyepka, M., Jerabek, P., Petrek, M. & Damborsky, J. (2006). Mechanism of enhanced conversion of 1,2,3-trichloropropane by mutant haloalkane dehalogenase revealed by molecular modeling. *J. Comput.-Aided Mol. Des.* **20**, 375–383.
41. Negri, A., Marco, E., Damborsky, J. & Gago, F. (2007). Stepwise dissection and visualization of the catalytic mechanism of haloalkane dehalogenase LinB using molecular dynamics simulations and computer graphics. *J. Mol. Graphics Modell.* **26**, 643–651.
42. Lüdemann, S. K., Lounnas, V. & Wade, R. C. (2000). How do substrates enter and products exit the buried active site of cytochrome P450cam? 2. Steered molecular dynamics and adiabatic mapping of substrate pathways. *J. Mol. Biol.* **303**, 813–830.
43. Li, W., Liu, H., Scott, E. E., Gräter, F., Halpert, J. R., Luo, X., Shen, J. & Jiang, H. (2005). Possible pathway (s) of testosterone egress from the active site of cytochrome P450 2B1: a steered molecular dynamics simulation. *Drug Metab. Dispos.* **33**, 910–919.
44. Dunn, A. R., Dmochowski, I. J., Bilwes, A. M., Gray, H.B. & Crane, B. R. (2001). Probing the open state of cytochrome P450cam with ruthenium-linker substrates. *Proc. Natl Acad. Sci. USA*, **98**, 12420–12425.
45. Yao, H., McCullough, C. R., Costache, A. D., Pullela, P. K. & Sem, D. S. (2007). Structural evidence for a functionally relevant second camphor binding site in P450cam: model for substrate entry into a P450 active site. *Proteins*, **69**, 125–138.
46. Podust, L. M., Poulos, T. L. & Waterman, M. R. (2001). Crystal structure of cytochrome P450 14α-sterol demethylase (CYP51) from *Mycobacterium tuberculosis* in complex with azole inhibitors. *Proc. Natl Acad. Sci. USA*, **98**, 3068–3073.
47. Seifert, A., Tatzel, S., Schmid, R. D. & Pleiss, J. (2006). Multiple molecular dynamics simulations of human P450 monooxygenase CYP2C9: the molecular basis of substrate binding and regioselectivity toward warfarin. *Proteins*, **64**, 147–155.
48. Prasad, S., Mazumdar, S. & Mitra, S. (2000). Binding of camphor to *Pseudomonas putida* cytochrome P450cam: steady-state and picosecond time-resolved fluorescence studies. *FEBS Lett.* **477**, 157–160.
49. Strasser, A. & Wittmann, H. (2007). LIGPATH: a module for predictive calculation of a ligand's pathway into a receptor-application to the gpH_1-receptor. *J. Mol. Model.* **13**, 209–218.
50. Kennes, C., Pries, F., Krooshof, G. H., Bokma, E., Kingma, J. & Janssen, D. B. (1995). Replacement of tryptophan residues in haloalkane dehalogenase reduces halide binding and catalytic activity. *Eur. J. Biochem.* **228**, 403–407.
51. Damborsky, J., Kuty, M., Nemec, M. & Koca, J. (1997). A molecular modelling study of the catalytic mechanism of haloalkane dehalogenase: 1. Quantum chemical study of the first reaction step. *J. Chem. Inf. Comput. Sci.* **37**, 562–568.
52. Damborsky, J. & Koca, J. (1999). Analysis of the reaction mechanism and substrate specificity of haloalkane dehalogenases by sequential and structural comparisons. *Protein Eng.* **12**, 989–998.
53. Schindler, J. F., Naranjo, P. A., Honaberger, D. A., Chang, C. H., Brainard, J. R., Vanderberg, L. A. & Unkefer, C. J. (1999). Haloalkane dehalogenases: steady-state kinetics and halide inhibition. *Biochemistry*, **38**, 5772–5778.
54. Marek, J., Vevodova, J., Smatanova, I. K., Nagata, Y., Svensson, L. A., Newman, J. *et al.* (2000). Crystal structure of the haloalkane dehalogenase from *Sphingomonas paucimobilis* UT26. *Biochemistry*, **39**, 14082–14086.
55. Bohac, M., Nagata, Y., Prokop, Z., Prokop, M., Monincova, M., Tsuda, M. *et al.* (2002). Halide-stabilizing residues of haloalkane dehalogenases studied by quantum mechanic calculations and site-directed mutagenesis. *Biochemistry*, **41**, 14272–14280.
56. Monincova, M., Prokop, Z., Vevodova, J., Nagata, Y. & Damborsky, J. (2007). Weak activity of haloalkane dehalogenase LinB with 1,2,3-trichloropropane revealed by X-ray crystallography and microcalorimetry. *Appl. Environ. Microbiol.* **73**, 2005–2008.
57. Streltsov, V. A., Prokop, Z., Damborsky, J., Nagata, Y., Oakley, A. & Wilce, M. C. J. (2003). Haloalkane dehalogenase LinB from *Sphingomonas paucimobilis* UT26: X-ray crystallographic studies of dehalogenation of brominated substrates. *Biochemistry*, **42**, 10104–10112.
58. Oakley, A. J., Klvana, M., Otyepka, M., Nagata, Y., Wilce, M. C. J. & Damborsky, J. (2004). Crystal structure of haloalkane dehalogenase LinB from *Sphingomonas paucimobilis* UT26 at 0.95 Å resolution: dynamics of catalytic residues. *Biochemistry*, **43**, 870–878.
59. Deprez, E., Gerber, N. C., Di Primo, C., Douzou, P., Sligar, S. G. & Hui Bon Hoa, G. (1994). Electrostatic control of the substrate access channel in cytochrome P450cam. *Biochemistry*, **33**, 14464–14468.
60. Di Primo, C., Deprez, E., Sligar, S. G. & Hui Bon Hoa, G. (1997). Origin of the photoacoustic signal in cytochrome P450cam: role of the Arg186-Asp251-Lys178 bifurcated salt bridge. *Biochemistry*, **36**, 112–118.
61. Lounnas, V. & Wade, R. C. (1997). Exceptionally stable salt bridges in cytochrome P450cam have functional roles. *Biochemistry*, **36**, 5402–5417.
62. Oprea, T. I., Hummer, G. & Garcia, A. E. (1997). Identification of a functional water channel in cytochrome P450 enzymes. *Proc. Natl Acad. Sci. USA*, **94**, 2133–2138.
63. Kovach, I. M., Qian, N. & Bencsura, A. (1994). Efficient product clearance through exit channels in substrate hydrolysis by acetylcholinesterase. *FEBS Lett.* **349**, 60–64.
64. Enyedy, I., Kovach, I. & Brooks, B. (1998). Alternate pathways for acetic acid and acetate ion release from acetylcholinesterase: a molecular dynamics study. *J. Am. Chem. Soc.* **120**, 8043–8050.
65. Ripoll, D. R., Faerman, C. H., Axelsen, P. H., Silman, I. & Sussman, J. L. (1993). An electrostatic mechanism for substrate guidance down the aromatic gorge of acetylcholinesterase. *Proc. Natl Acad. Sci. USA*, **90**, 5128–5132.
66. Van Belle, D., De Maria, L., Iurcu, G. & Wodak, S. J. (2000). Pathways of ligand clearance in acetylcholinesterase by multiple copy sampling. *J. Mol. Biol.* **298**, 705–726.
67. Xu, Y., Shen, J., Luo, X., Silman, I., Sussman, J. L., Chen, K. & Jiang, H. (2003). How does huperzine a enter and leave the binding gorge of acetylcholinesterase? Steered molecular dynamics simulations. *J. Am. Chem. Soc.* **125**, 11340–11349.
68. Khajehpour, M., Rietveld, I., Vinogradov, S., Prabhu, N. V., Sharp, K. A. & Vanderkooi, J. M. (2003). Accessibility of oxygen with respect to the heme pocket in horseradish peroxidase. *Proteins*, **53**, 656–666.
69. Zelent, B., Kaposi, A., Nucci, N., Sharp, K., Dalosto, S., Wright, W. & Vanderkooi, J. (2004). Water channel

of horseradish peroxidase studied by the charge-transfer absorption band of ferric heme. *J. Phys. Chem. B*, **108**, 10317–10324.
70. Teeter, M. M. (2004). Myoglobin cavities provide interior ligand pathway. *Protein Sci.* **13**, 313–318.
71. Bui, J. M., Henchman, R. H. & McCammon, J. A. (2003). The dynamics of ligand barrier crossing inside the acetylcholinesterase gorge. *Biophys. J.* **85**, 2267–2272.
72. Ye, X., Yu, A. & Champion, P. M. (2006). Dynamics of nitric oxide rebinding and escape in horseradish peroxidase. *J. Am. Chem. Soc.* **128**, 1444–1445.
73. Henchman, R. H., Tai, K., Shen, T. & McCammon, J. A. (2002). Properties of water molecules in the active site gorge of acetylcholinesterase from computer simulation. *Biophys. J.* **82**, 2671–2682.
74. Zwanzig, R. (1992). Dynamical disorder: passage through a fluctuating bottleneck. *J. Chem. Phys.* **97**, 3587–3589.
75. Carugo, O. & Argos, P. (1998). Accessibility to internal cavities and ligand binding sites monitored by protein crystallographic thermal factors. *Proteins*, **31**, 201–213.
76. Cohen, J., Arkhipov, A., Braun, R. I. & Schulten, K. (2006). Imaging the migration pathways for O_2, CO, NO, and Xe inside myoglobin. *Biophys. J.* **91**, 1844–1857.
77. Lavalette, D., Tétreau, C. & Mouawad, L. (2006). Ligand migration and escape pathways in haem proteins. *Biochem. Soc. Trans.* **34**, 975–978.
78. Maniatis, T., Fritsch, E. F. & Sambrook, J. (1982). *Molecular Cloning: A Laboratory Manual.* Cold Spring Harbor Laboratory Press, Cold Spring Harbor, NY.
79. Stsiapanava, A., Koudelaková, T., Lapkouski, M., Pavlova, M., Damborsky, J. & Smatanova, I. K. (2008). Crystals of DhaA mutants from *Rhodococcus rhodochrous* NCIMB13064 diffracted to ultrahigh resolution: crystallization and preliminary diffraction analysis. *Acta Crystallogr., Sect. F*, **64**, 137–140.
80. Andrade, M. A., Chacon, P., Merelo, J. J. & Moran, F. (1993). Evaluation of secondary structure of proteins from UV circular dichroism spectra using an unsupervised learning neural network. *Protein Eng.* **6**, 383–390.
81. Sreerama, N. & Woody, R. W. (1993). A self-consistent method for the analysis of protein secondary structure from circular dichroism. *Anal. Biochem.* **209**, 32–44.
82. Deleage, G. & Geourjon, C. (1993). An interactive graphic program for calculating the secondary structure content of proteins from circular dichroism spectrum. *Comput. Appl. Biosci.* **9**, 197–199.
83. Iwasaki, I., Utsumi, S. & Ozawa, T. (1952). New colorimetric determination of chloride using mercuric thiocyanate and ferric ion. *Bull. Chem. Soc. Jpn.* **25**, 226.
84. DeLano, W. (2002). *The PyMOL Molecular Graphics System.* DeLano Scientific, Palo Alto, CA.
85. Stewart, J. J. (1990). MOPAC: a semiempirical molecular orbital program. *J. Comput.-Aided Mol. Des.* **4**, 1–105.
86. Frisch, M. J., Trucks, G. W., Schlegel, H. B., Gill, P. M. W., Johnson, B. J., Robb, M. A. *et al.* (1995). Gaussian 94, Revission D.4 Gaussian, Inc., Pittsburgh, PA.
87. Case, D. A., Darden, T. A., Cheatham, T. E., Simmerling, C. L., Wang, J., Duke, R. E. *et al.* (2004). AMBER 8 University of California, San Francisco, CA.
88. Morris, G. M., Goodsell, D. S., Halliday, R. S., Huey, R., Hart, W. E., Belew, R. K. & Olson, A. J. (1998). Automated docking using a Lamarckian genetic algorithm and an empirical binding free energy function. *J. Comput. Chem.* **19**, 1639–1662.
89. Vriend, G. (1990). WHAT IF: a molecular modeling and drug design program. *J. Mol. Graphics*, **8**, 52–56.
90. Cornell, W., Cieplak, P., Bayly, C., Gould, I., Merz, K., Ferguson, D. *et al.* (1996). A second generation force field for the simulation of proteins, nucleic acids, and organic molecules. *J. Am. Chem. Soc.* **118**, 2309.
91. Jorgensen, W. L., Chandrasekhar, J., Madura, J. D., Impey, R. W. & Klein, M. L. (1983). Comparison of simple potential functions for simulating liquid water. *J. Chem. Phys.* **79**, 926–935.
92. Berendsen, H. J. C., Postma, J. P. M., van Gunsteren, W. F., DiNola, A. & Haak, J. R. (1984). Molecular dynamics with coupling to an external bath. *J. Chem. Phys.* **81**, 3684–3690.
93. Ryckaert, J., Ciccotti, G. & Berendsen, H. J. C. (1977). Numerical integration of the cartesian equations of motion of a system with constraints: molecular dynamics of *n*-alkanes. *J. Comput. Phys.* **23**, 327–341.
94. Kabsch, W. & Sander, C. (1983). Dictionary of protein secondary structure: pattern recognition of hydrogen-bonded and geometrical features. *Biopolymers*, **22**, 2577–2637.
95. Humphrey, W., Dalke, A. & Schulten, K. (1996). VMD: visual molecular dynamics. *J. Mol. Graphics*, **14**, 33–38.
96. Onufriev, A., Bashford, D. & Case, D. A. (2004). Exploring protein native states and large-scale conformational changes with a modified generalized Born model. *Proteins*, **55**, 383–394.